ISSN: 2994-7510

Research Article

Journal of Water Research

Assessing the Effect of Change in Climate and Land Use has on Groundwater Recharge Suitability in the Thiba River Sub Basin, Kenya

Abel M. Omanga[1]*, Arthur W. Sichangi[1], Godfrey O. Makokha[2] and Ruth N. Waswa[3]

[1]*Institute of Geomatics, GIS & Remote Sensing (IGGReS), Dedan Kimathi University of Technology, Private Bag 10143 Nyeri-Mweiga road, Nyeri-Kenya*

[2]*School of Science and Informatics, Taita Taveta University, P. O. Box 635, Voi 80300, Kenya*

[3]*Department of Earth and Climate Science, Faculty of Science and Technology, University of Nairobi, P.O Box 30197, Nairobi, Kenya*

***Corresponding Author**
Abel M. Omanga, Institute of Geomatics, GIS & Remote Sensing (IGGReS), Dedan Kimathi University of Technology, Private Bag 10143 Nyeri-Mweiga road, Nyeri-Kenya.

Submitted: 2024, Dec 01; **Accepted:** 2024, Dec 26; **Published:** 2025, Jan 10

Citation: Omanga, A. M., Sichangi, A. W., Makokha, G. O., Waswa, R. N. (2024). Assessing the Effect of Change in Climate and Land Use has on Groundwater Recharge Suitability in the Thiba River Sub Basin, Kenya. *J Water Res,* 3(1), 01-22.

Abstract

Groundwater recharge Suitability (GWRS) mapping is a critical step towards planning for groundwater management and development. This study sought to assess the influence of change in climate and land use on the spatial-temporal variability of groundwater recharge suitability areas in Thiba river sub basin. The study applied the multi-influencing factor (MIF) technique to delineate the GWRS zones in Thiba river sub basin in three instances, historical (1986), current (2020), and future (2050) period. Water availability for the various uses within Thiba river sub basin is uncertain in the dry season, attributed to resource degradation due to over-exploitation and limited investments. Over-reliance on surface water with poor development of groundwater that is allocated without detailed quantification and quality assessment causing resource degradation. Future climate projections were derived from the Coordinated Regional Downscaling Experiment (CORDEX) for the African region under two Representative Concentration Pathways (RCP 4.5). Ground water recharge potential was assessed using a Multi-Influencing Factor (MIF) technique using Slope, Land use, Rainfall, lithology, landforms, Drainage density, Lineament density and soil as assessment parameters. Land cover images for the year 1986, 2003 and 2020 were classified into 6 land uses; bare, Built-up, cropland, forest, Grassland and Wetland areas and used to project land use in 2050 using the CA-Markov model. Results indicate that climate change will significantly impact water. Detailed study linking groundwater recharge and groundwater yields is recommended to better inform resource managers on the level of quantitative groundwater variability over space.

Keywords: Recharge Suitability, Water Variability, Climate Change

1. Introduction

Sub–Saharan Africa is facing rapid rise in population and economic development. These two phenomena are characterized by anthropogenic activities that increasingly demand more water. Water Resources are, on the contrary, rapidly degrading in quality and quantity leading water uncertainty across since they can't meet the demand [1]. Water scarcity is threatening many countries. By mid-century urban water needs shall rise by 80% and general global water demand by 50%, rendering about four Billion people in the world at water access risk. The production of energy and food shall rapidly increase. According to Floerke, (2018) more than 27% of the world's cities will face water scarcity and potentially 19% of them will depend on inter-basin transfers from outside their territory. Surface water dominates water sources for the majority of Sub-Saharan Africa despite threats facing these resources.

Water resources need proper management for sustainability. Kenya's temperature has risen by about 1.0 °C since 1960. Rainfall patterns have changed and become unreliable. Mt. Kenya national park and Aberdare forests form the origin of two major river systems in Kenya. The rivers are Tana and Ewaso Nyiro, draining about three-quarters of the country's surface area. River Tana provides water to about 50% of the country's population. Tana river serves various water uses; irrigation, hydro-electric power generation, commercial use, tourism, livestock, industrial, domestic use, and public water. The Discharge of river Tana ranges between 60 and 750m3 s-1. The lower slopes of Mt. Kenya are incised to depths of 600ft by a network of radial streams. The high average annual rainfall has resulted in a dense network of parallel streams forming steep-sided interfluves. The drainage variation in their physiography results from the varying nature and age of the underlying

geological structure.

The older volcanic are deeply dissected resulting in the obvious conspicuous valleys with steep walls that characterize the western slope streams such as Thiba, Rupingazi and Nyamindi [2]. Thiba sub-basin is vital in supplying water to the Mwea Irrigation Scheme. It also supports other water demands, hydropower, domestic and industrial. Some of the major human activities include two upcoming micro-hydro plants. The Main problem currently facing the community, is fluctuating streamflow availability leading to inequitable access to water. However, groundwater remains to be largely undeveloped across the country (USAID and SWP, 2021). The study used the multi-Influencing Factors (MIF) technique to assess the variability of GWRS zones in response to change in land use and climate.

2. Study Area Characteristics

The study is in Tana basin area in Thiba river sub basin which traverse Kirinyaga and Embu counties at the slopes of Mount Kenya. The Thiba river sub-basin is divided into the lowest unit of catchment management called a sub catchment. It is located between 37°10'30"E and 37°28'0"E, 0°43'30"S and 0°10'0"S with an aerial coverage of 1,525 km2, which makes up 1.2 % of the entire Tana Basin. The study area falls into three ecological zones: the lowland areas (1158-2000) metres above sea level, midland areas (2000-3400) metres above sea level and the highland area (3,400 – 5380) metres above sea level.

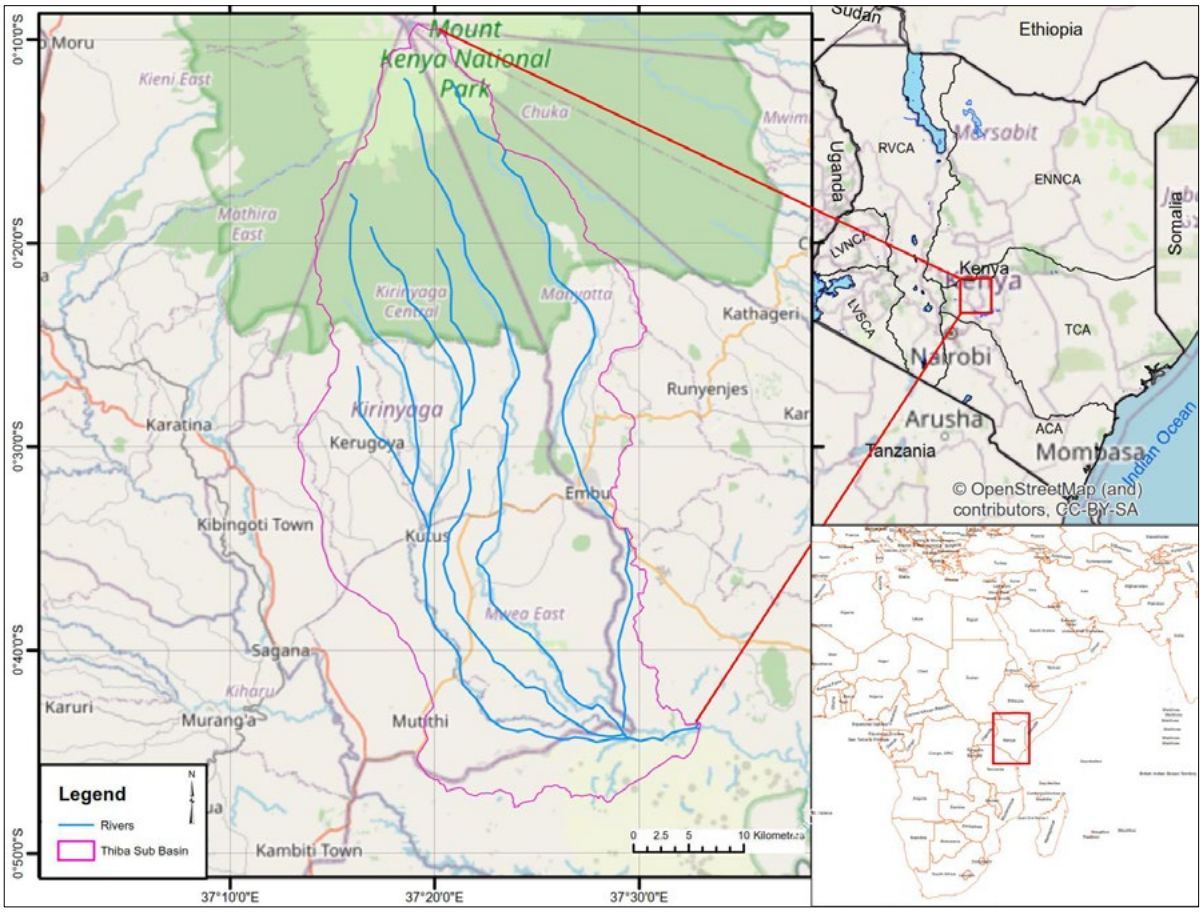

Figure 1: Thiba River Sub Basin, Physical Location, and Basin Area Overview for Kenya

It has a mean elevation ranging 1,158m to 5,380 m above sea level [2]. The sub basin receives long rain between March to May while short rains come between September to November. The peak rainfall of about 300 mm and 250 mm fall in April and November respectively with the lowest temperatures of 16oC recorded in July. The lower zones have a mean evapotranspiration potential of 1700mm compared to below 500mm in the upper zones [3]. Significant variation between rain and temperature is observed longitudinally. Mt. Kenya volcanics comprise the Mt Kenya Volcanics (North and South) and the Nyambene and the Eastern basement Volcanics. The Mt Kenya Volcanics on the northern side comprise mugearites, phonolites, basalts and trachytic tuffs interspersed by mudflows. The Southern volcanics has the uppermost units consist of ash accumulations, bedded deposits containing abundant lava and pumice inclusions of all sizes, with fragments of feldspars, nepheline, and dark minerals, in a fine-grained matrix underlain by micro porphyritic. The Eastern Basement is composed of banded biotite/muscovite/hornblende gneisses; hornblende schists, granitoid gneisses. The gneisses and schists are of semi-pelitic and pelitic origin. Bands of crystalline limestone and calc-silicate gneisses occur.

The study area is a climatically homogenous region sitting in the windward region of Mt. Kenya with two distinct seasons that align with the findings in this study [4]. The Upper Tana region has two seasons, wet and dry seasons that are characterized by significant spatial variation in precipitation [22]. The rainfall patterns are highly influenced by the relief features of the area

and the influence of the North-South movement of the zonal arm of the Inter-Tropical Convergence Zone [5]. The rainfall pattern is bimodal in seasons but locally vary in space. The study area has significant topographic variation that rise from 1158m to 5380m above sea level. The seasonal pattern is same, but rainfall distribution is greatly varied from the mountain peak of Mt. Kenya that receive about 1600mm/year to the Mwea plains that receive an average of 968mm/year [5,3]. The low rainfall and high temperatures recorded in the lower zone of the study area, areas around Mwea irrigation scheme are associated with the influence of the adjacent arid region that characterize the Athi basin and the low-lying basin like topography with dry winds most of the time in the year. Long term average of rainfall between the year 1986 up to 2020 show the lowland zone in the study area registering rainfall of 1160mm/yr and maximum temperature of about 19.20C in comparison to the highland that register a long-term average rainfall of 1550mm/yr and a maximum temperature of 16.40C [3].

3. Materials and Methods

3.1 Data Preparation

Remote sensing data and field collected data were used to map the GWRP zones. Table 1 gives a summary of the data used for the study and their sources.

Data Type	Source	Format	Code
Drainage density	Developed from Shuttle Radar Topography Mission (SRTM) DEM (USGS), Resolution: 30 m	Raster	Dd
Slope	Developed from SRTM data (resolution: 30 m)	Digital	SL
Rainfall (1986, 2020 and 2050)	WCRP CORDEX	Tabular	Rf
Land use	Prepared from Landsat 4-5(TM), and Landsat 8(OLI) 30m Spatial resolution	Raster	Lu
Soil (Soil texture)	International Livestock Research Institute	Digital	St
Lineament Density	Digitised from raster maps obtained from National Geodata Centre (NGDC) for Kenya	Digital	Ld
Geology	Digitised from raster maps obtained from National Geodata Centre (NGDC) for Kenya	Digital	Lt
Groundwater Levels	Water resources Authority	Digital	GL
Landforms	harvard-africover-ke-lndfrm.	Digital	Lf

Table 1: Data Types, Sources and Product Code Adopted for the Study.

3.1.1 Rainfall and Temperature

The study used 0.25º x 0.25º gridded monthly Climate Hazard Group Infrared Precipitation with Stations (CHIRPS) and the fifth generation ECMWF reanalysis global climate (ERA5) datasets from 1986 to 2020 for the entire study. Details of these datasets can be found in [6,7]. CORDEX model outputs were downscaled to 25Km resolution and on a monthly timescale was used to project climate over the Thiba river Sub-basin until the year 2050. Two scenarios were considered; RCP4.5 and RCP8.5. Linear Scaling of precipitation and temperature was used to correct for biases in the climate models. Several statistics were used to evaluate Models before further analysis which were correlation analysis, RMSE, standard deviation and model bias. More details about these statistics and bias correction methods can be found in [1]. The available observed data was correlated with the gridded data to assess the performance over the study area and high correlation coefficients of 0.85, 0.82 and 0.69 were observed for rainfall, maximum and minimum temperature respectively. Climate projections were obtained from the World Climate Research Project (WCRP) domain (https://www.wcrp-climate.org/), accessed on June 14th, 2022. The data was rasterized using the linear kriging interpolation method.

3.1.2 Geology

Geological map of the area was generated by assembling existing geological maps of scale 1:125,000 obtained from the National Geodata Centre (NGDC) for Kenya. The maps were scanned, georeferenced and digitized in QGIS desktop environment. Data used is indicated in table 2.

Type	Symbol	Description	Group	Weight
Quaternary deposits (Poorly sorted)	Q	Alluvium and aeolian deposits. The uppermost units consist of ash accumulations, bedded deposits containing abundant lava and pumice inclusions of all sizes, with fragments of feldspars, nepheline, and dark minerals, in a fine-grained matrix. These are underlain by micro porphyritic. <240m3/day.	Medium	3
Volcanics	Ti	Holocene – Basalt flows, pyroclastics.	Low	2
Metamorphics	PC	Precambrian -Banded biotite/ muscovite/ hornblende gneisses; hornblende schists, granitoid gneisses. The gneisses and schists are of semi-pelitic and pelitic origin. Bands of crystalline limestone and calc-silicate gneisses occur; high-grade metamorphism has resulted. >86m3/day.	Very Low	1

Table 2: The Weights Allocated to the Geological Composition in the Area.

3.1.3 Lineament Density

Lineament data was digitized from geological maps. Faults were converted to raster using Rasterize (vector to Raster) under Conversion of GDAL tools in QGIS and then reclassified. Lineament density was calculated from linear structures digitized from the Geological Map of Kenya with Structural Contours (BEICIP, 1987) [8]. The study used lineament-length density (Ld) after which represents the total length of lineaments in a unit area, as shown in equation 1:

$$L_d = \frac{\sum_{i=1}^{i=n} L_i}{A} \ldots\ldots\ldots\ldots\ldots\ldots \quad (1)$$

where $\sum_{i=1}^{i=n} L_i$ denotes the total length of lineaments, and A denotes the unit area.

A high L_d value infers high secondary permeability, thus indicating a zone with greater potential for groundwater rechargeability for the same rock type. Lineament density range was classified into 3 groups – high, moderate, and low.

3.1.4 Landforms

The topography was classified as lowlands, midlands and uplands using the landform layer obtained from; https://maps.princeton.edu/catalog/harvard-africover-ke-lndfrm. The study area was categorized into lowland (1,130-1180), midland (1180-1750) and highland (1750 – 4750) meters above sea level. The classification is based on the agro-ecological zonation for Upper Tana (ISRIC, 2023).

3.1.5 Slope

The slope factor was calculated using the 30 m DEM based on the maximum rate of percentage change in value from each cell to neighbouring cells [1].

3.1.6 Drainage Density

Drainage density (D) is defined as the closeness of spacing of stream channels calculated as the measure of the total length of the stream segment of all orders per unit distance [9]. The drainage density was represented by the following equation: The drainage density was generated indirectly from the slope as shown in equation 2.

$$Db = L/A \ldots\ldots\ldots\ldots\ldots \quad (2)$$

Where: Db = Drainage Density, L = Total Length of all Stream Channel and A = Area of Basin.

3.1.7 Soil

Soil map of the area was downloaded in digital form from the ILRI data portal. The soil was categorized into texture types.

3.1.8 Land Use (LU)

Raw satellite imagery was from LANDSAT repository for Landsat 4-5(TM), and Landsat 8(OLI) 30m. The images were classified into 6 classes for the years 1986, 2003 and 2020. The classes included bare, Built-up, cropland, forest, Grassland and Wetland areas using level 1 scheme of classification suggested by [10]. Accuracy assessment was done by comparing classified to ground referenced data captured by GPS device and using the confusion matrix [11]. Land cover change prediction has two aspects: the quantity of change as provided by the Markov change model matrix and the spatial distribution of change given by multilayer perceptron neural network (MLPNN). Land cover maps were predicted for 2050 using transition maps from 1986-2003-2020.

3.1.9 Groundwater Levels

Borehole abstraction and borehole completion record data was obtained from the Water Resources Authority. The two were linked to obtain groundwater levels that were rasterized using linear kriging interpolation method.

3.1.10 Parameter Rating for Weighted Overlay

Tables 3 and Table 4 show the parameter rating for weighted overlay before and after sensitivity analysis respectively.

Factor	Domain Effect	Domain Weight	Epoch	Allocated Rate of influence / Parameter	Calculation process for % rate	Percentage Rate of influence/ factor
Lineament Density	6 – 15km/km2	3				
	2 – 6 km/km2	2		1.5	(1.5/18) * 100	8.33
	0-2 km/km2	1	N/A			
Rainfall	998 - 1115	1				
	1115 - 1217	2	1986			
	1217 - 1322	3				
	1322 - 1434	4				
	1434 - 1566	5				
	724-876	1				
	876-1070	2				
	1070-1380	3		2.5	(2.5/18) * 100	13.89
	1380-1675	4	2020			
	1675-1903	5				
	1071 - 1189	1				
	1189 - 1300	2				
	1300 - 1414	3				
	1414 - 1513	4	2050			
	1513 - 1618	5				
Soil	Loamy	2	N/A	1	(1.0/18) * 100	5.56
	Clayey	1				
Drainage Density	0-4	5				
	04-12	4				
	12-23	3	N/A	1.5	(1.5/18) * 100	8.33
	23-39	2				
	39-65	1				
Lithology	Quaternary deposits (Poorly sorted)	3				
	Volcanics	2		2.5	(2.5/18) * 100	13.89
	Metamorphics	1	N/A			
Slope	0-5.22	5				
	5.22-12.46	4				
	12.46-22.5	3		4	(4/18) * 100	22.22
	22.5-38.18	2				
	38.18-102.47	1				
Land use	Forest	6				
	Grassland	5				
	Cropland	4		3	(2.5/18) * 100	16.67
	Wetland	3				
	Bare	2				
	Built Up	1				
	Forest	6				
Landforms	Hills and Mountain Foot ridges	1				
	Mountains	2		2	(2/18) * 100	11.11
	Plain	3				
				Σ18		100.00

Table 3: Parameter Rating Before Sensitivity Analysis

Factor	Domain Effect	Domain Weight	Epoch	Allocated Rate of influence / Parameter	Calculation process for % rate	Percentage Rate of influence/ factor
Lineament Density	6 – 15km/km2	3				
	2 – 6 km/km2	2		1.2	(1.2/16.1) * 100	7.45
	0-2 km/km2	1	N/A			
Rainfall	998 - 1115	1				
	1115 - 1217	2	1986			
	1217 - 1322	3				
	1322 - 1434	4				
	1434 - 1566	5				
	724-876	1				
	876-1070	2				
	1070-1380	3		2.5	(2.5/16.1) * 100	15.53
	1380-1675	4	2020			
	1675-1903	5				
	1071 - 1189	1				
	1189 - 1300	2				
	1300 - 1414	3				
	1414 - 1513	4	2050			
	1513 - 1618	5				
Soil	Loamy	2	N/A	1	(1.0/16.1) * 100	6.21
	Clayey	1				
Drainage Density	0-4	5				
	04-12	4				
	12-23	3	N/A	1.4	(1.4/16.1) * 100	8.70
	23-39	2				
	39-65	1				
Lithology	Quaternary deposits (Poorly sorted)	3				
	Volcanics	2		2	(2.0/16.1) * 100	12.42
	Metamorphics	1	N/A			
Slope	0-5.22	5				
	5.22-12.46	4				
	12.46-22.5	3		3.5	(3.5/16.1) * 100	21.74
	22.5-38.18	2				
	38.18-102.47	1				
Land use	Forest	6				
	Grassland	5				
	Cropland	4		3	(2.5/16.1) * 100	18.63
	Wetland	3				
	Bare	2				
	Built Up	1				
	Forest	6				
Landforms	Hills and Mountain Foot ridges	1				
	Mountains	2		1.5	(1.5/16.1) * 100	9.32
	Plain	3				
				Σ16.1		100.00

Table 4: Parameter Rating After Sensitivity Analysis and Weight Adjustment

3.2 Methods

3.2.1 Multi-Influencing Factors (MIF)

Groundwater recharge potential zones were mapped using the Multi-Influencing Factors (MIF) technique using eight factors, namely: Rainfall, Lineament density, Slope, Drainage density, Land use/land cover, Lithology, landforms, and Soil type layers. MIF is a widely used MCDM technique for environmental management.

The procedure for mapping groundwater Recharge Zones using the weighted overlay tool of weighted Overlay analysis tool of QGIS 3.18. The thematic layers were converted into standard 1km2 grid raster. The calculation was done by multiplying individual cell factor cell values with the assigned weight and summing together the values of all layers for every cell to produce the groundwater recharge potential map. Equation 3 shows the ground water recharge potential weighted overlay equation [12].

$$GWRS = \sum_{i=0}^{n} W_i XR_i$$
$$= (LI_c LI_w + LULC_c LULC_w + SLO_c SLO_W + GM_C GM_w + LD_C LD_w + RF_C RF_w + DD_C DD_w + SL_C SL_W) \ldots\ldots\ldots\ldots\ldots\ldots (3)$$

Where Groundwater Recharge Suitability (GWRS) is the Groundwater recharge suitable zone, W_i is the weight of every thematic layer, R_i is the rating of each class in every thematic layer. LI is the lithology of the aquifer, LU/LC is the land-use/ land-cover, SLO is the slope, LD is the lineament, RF is the rainfall, DD is the drainage density, GM is the geomorphology/ Landforms and SL is the soil cover. The subscripts ***c*** and ***w*** refer, respectively, to the factor class of a thematic layer and its percentage influence on recharge. This means each class rank is multiplied by the layer weight to obtain the position for the layer in the overlay analysis [12]. Figure 2 shows the flow chart methodology for mapping recharge suitability.

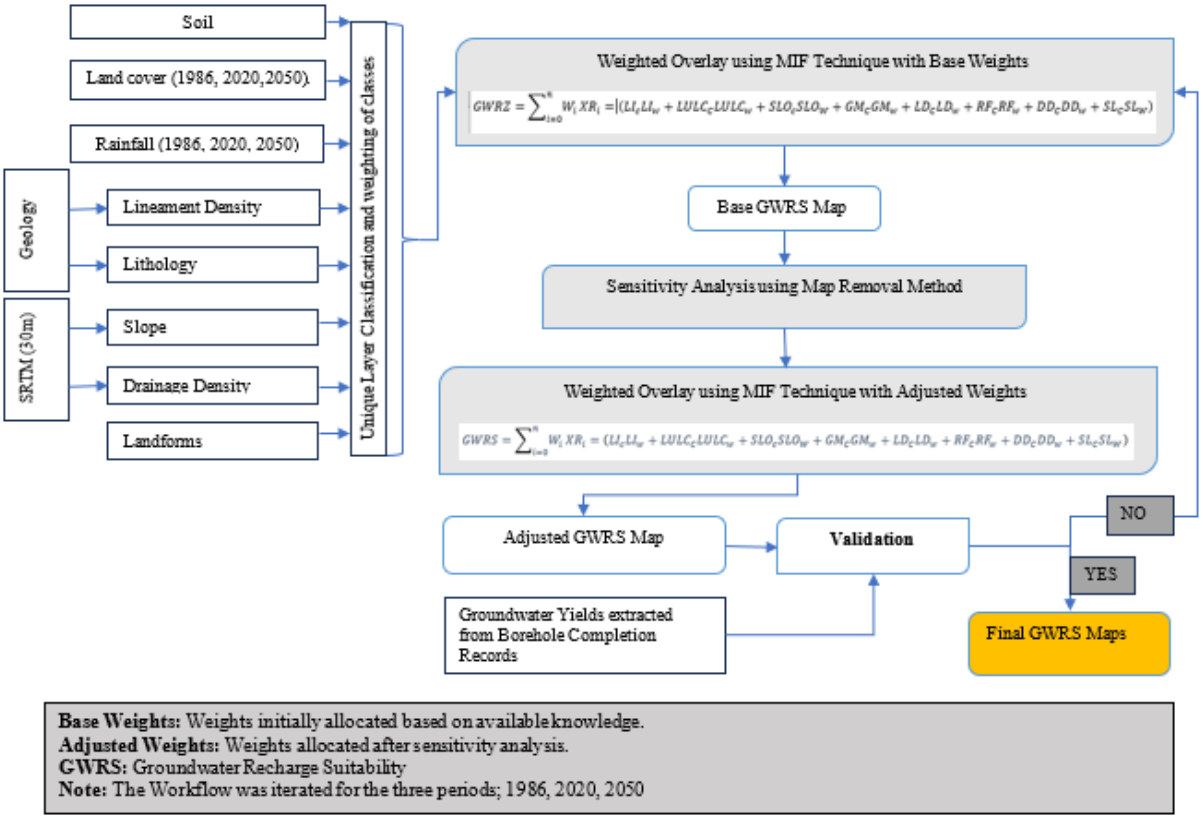

Figure 2: Methodology for Mapping Groundwater Recharge Suitability Assessment

***GWRS**: Groundwater Recharge Suitability, **LULC**: Land use Land cover, **RF**: Rainfall, **LI**: Lithology, **LD**: Lineament Density, **SLO**: Slope, **St**: Soil Texture, **GM**: Geomorphology/Landforms, **DD**: Drainage Density, SL: Soil

3.2.2 Raster Reclassification

The Raster maps were processed at a standard one kilometer (1000m X1000m) square raster grids; The overlay was done based on Weighted Overlay sum (Spatial Analysis), which considers data set influence of each layer.

3.2.3 Estimating Relative Weights

Weights were assigned to variables based on expert opinion and past study recommendations on their influence on groundwater storage and flow. The weights were categorized as minor (0.5) or major (1). The total weights assigned through a pairwise comparison was normalized by diving the variable total weight by the cumulative variable weight (Equation 4).

$$X_{ij} = \frac{C_{ij}}{L_{ij}} \ldots\ldots\ldots\ldots\ldots\ldots \quad (4)$$

where X_{ij} is normalized pair-wise matrix value at i_{th} row and j_{th} column, C is the value assigned to each criterion at I_{th} row and j_{th} column and L_{ij} is the total values in each column of the pair-wise matrix.

This rate was converted to a percentage using Equation 5, the outcome in Table 5.

$$Score = \frac{(Major\ effect + Minor\ effect)}{\sum(Major\ effect + Minor\ effect)}\ X\ 100 \ldots\ldots\ldots\ldots\ldots\ldots (5)$$

3.2.4 Graphical Pairwise Comparison of Variables

The variables were compared using the graphical method as indicated in figure 3.

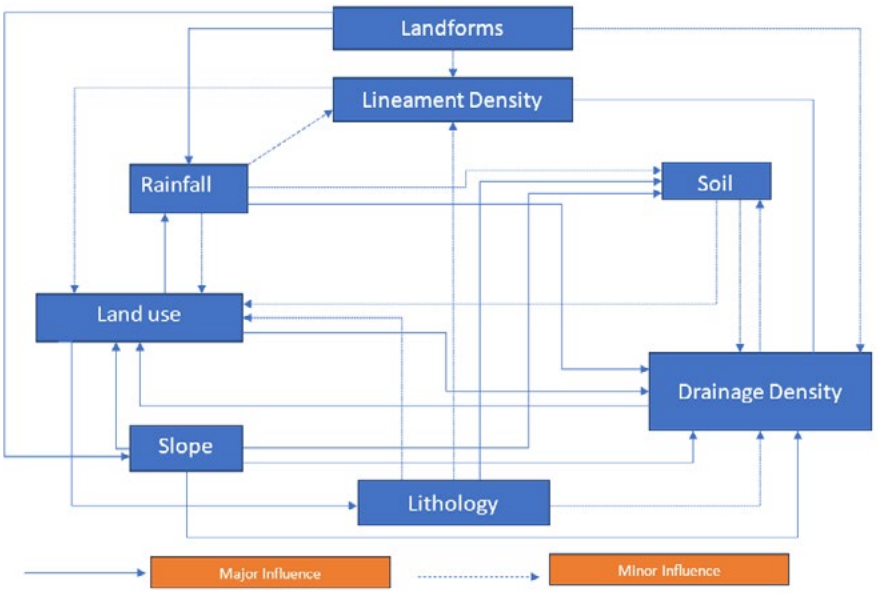

Figure 3: Pairwise Variable Analysis on their Influence on Groundwater Recharge Suitability

Factor	SUM-Major relation	Singular Weight (major)	Sum-Minor relations	Singular Weight (minor)	Calculation process for singular factor influence	Cumulative Weight/ factor	Calculation process for % rate	Percentage Rate of influence / factor
Lineament Density	1.00	1.00	1.00	0.50	(1x1) +(1x0.5)	1.50	(1.5/18) * 100	8.33
Rainfall	1.00	1.00	3.00	0.50	(1x1) +(3x0.5)	2.50	(2.5/18) * 100	13.89
Soil	0.00	1.00	2.00	0.50	(0x1) +(2x0.5)	1.00	(1.0/18) * 100	5.56
Drainage Density	1.00	1.00	1.00	0.50	(1x1) +(1x0.5)	1.50	(1.5/18) * 100	8.33
Lithology	1.00	1.00	3.00	0.50	(1x1) +(3x0.5)	2.50	(2.5/18) * 100	13.89
Slope	4.00	1.00	0.00	0.50	(4x1) +(0x0.5)	4.00	(4.0/18) * 100	22.22
Land use	3.00	1.00	0.00	0.50	(3x1) +(0x0.5)	3.00	(3.0/18) * 100	16.67
Landforms	1.00	1.00	2.00	0.50	(1x1) +(2x0.5)	2.00	(2.0/18) * 100	11.11
						Σ18		100.00

Table 5: Weights Assigned to Variables Influencing Groundwater Recharge Through Pairwise Comparison

3.2.5 Land Use Classification

a) Classification Scheme

Selection of a classification scheme preceded the image classification. The land cover classes (Table 6) that were adopted were level 1 modified USGS land use / land cover system suggested by Anderson, (1976).

Main class	Description
Agriculture land	Agricultural Land may be defined broadly as land used primarily for production of food and fibre. This category includes Cropland and Pasture, Ornamental Horticultural Areas.
Forest	Forest Lands have a tree-crown areal density (crown closure percentage) of 10 % or more, are stocked with trees capable of producing timber or other wood products and exert an influence on the climate or water regime. Forestlands include Deciduous, Evergreen and Mixed Forestlands.
Settlement/ built up	This comprises of areas of intensive use with much of the land covered by structures. Included in this category are cities, towns, villages, highways and transportation, power, and communications facilities.
Grassland/ Rangeland	Land where the potential natural vegetation is predominantly grasses, grass like plants, forbs, or shrubs.
Barren land	Barren Land is land of limited ability to support life and in which less than one third of the area has vegetation or other cover.

Table 6: Land Cover Classification System (source: anderson et al., (1976) Land Use Classification)

The study used Landsat sensor images at a spatial resolution of 30- meters (1986, 2003 and 2020). Image classification was supervised classification using the maximum likelihood according to Ohana-Levi and which have also been utilized by Murunga. Visual accuracy assessment was done by comparing classified to ground referenced data captured by GPS device and using high resolution Google Earth imagery. Systematic accuracy assessment was performed using the confusion matrix [11]. Overall accuracy and Kappa statistics were used to assess the accuracy of classification. Summary of steps of LULC classification and projection are as presented in Figure 4.

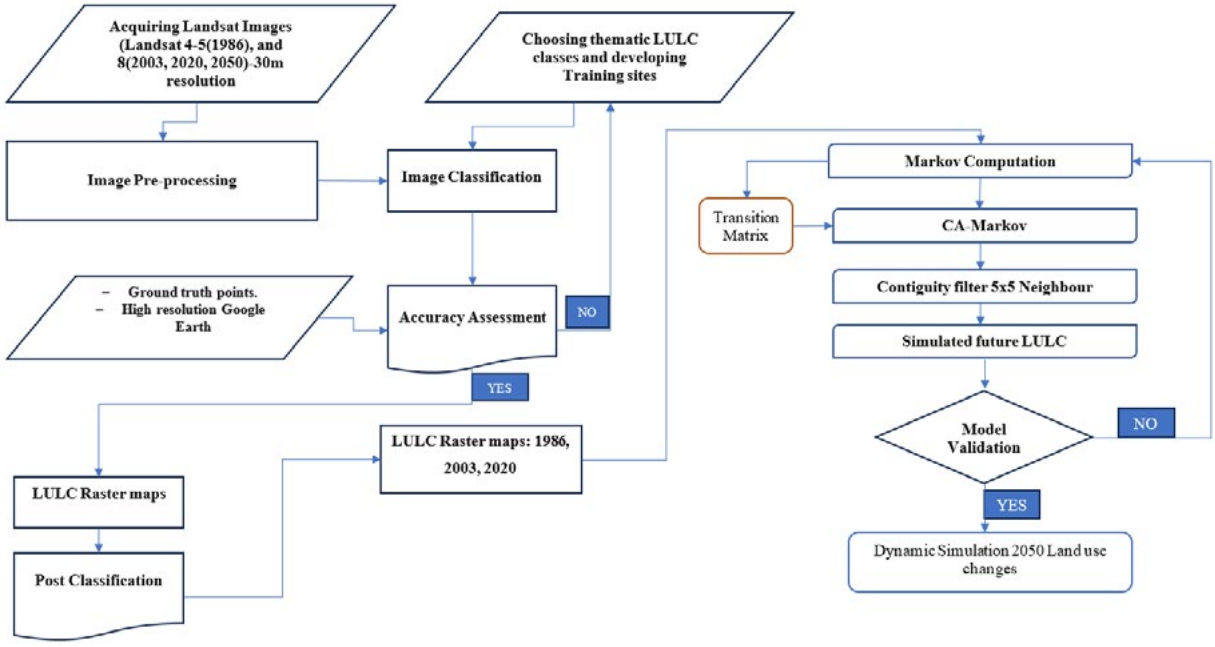

Figure 4: Land Use Classification and Prediction up to 2050 Using Ca-Markov Algorithm

b) Landcover Prediction

Land cover change prediction has two aspects: the quantity of change as provided by the Markov change model matrix and the spatial distribution of change given by multilayer perceptron neural network (MLPNN). Land cover provides the quantity of change by evaluating the Markov matrix comparing the initial (T1) and second land cover (T2), and then predicts the future land cover (T3) using a transition probability matrix for the future. The transition probability matrix displays the probability of each land cover category changing into another category. A value close to 0 indicates a low conversion probability, and 1 indicates a high conversion probability for the target land cover. Land

cover maps were predicted for 2050 using transition potential maps from 2003-2020. The agreement of the two categorical maps was measured by using Validate Tool in Idrisi Selva. The model is regarded to be validated if the Kstandard (overall kappa) score exceeds 70%. The values of k-index greater than 80% show good agreement between the projected and actual LULC map that exceeds the minimum acceptable standard. All indices are greater than 80%, showing a good overall agreement and projection ability of the model.

(i) The Markov Model

Equation (6) explains the calculation of the prediction of land use changes:

$$S(t_{t+1}) = P_{ij}\, x\, S(t) \ldots\ldots\ldots\ldots\ldots\ldots \quad (6)$$

where S (t) is the system status at time of t, S (t + 1) is the system status at time of t + 1; P_{ij} is the transition probability matrix in a state which is calculated as follows [13].

$$P = \|P_{ij}\| = \begin{Vmatrix} P_{1,1} & P_{1,2} \ldots & P_{1,N} \\ P_{2,1} & P_{2,2} \ldots & P_{2,N} \\ \ldots & \ldots & \ldots \\ P_{N,1} & P_{N,2} \ldots . & P_{N,N} \end{Vmatrix} (0 \le P_{ij} \le 1) \ldots\ldots\ldots\ldots\ldots\ldots (7)$$

P is the transition probability; P_{ij} stands for the probability of converting from current state I to another state j in next time; P_N is the state probability of any time. Low transition will have a probability near (0) and high transition have probabilities near (1).

Markov chain enables the prediction of LULC change through transition probabilities files which are matrices that record the probability that each land cover class will change to every other class. Through the Markov chain modelling, the analysis of two different dates of the LULC images induces the transition matrices, a transition area matrix, and a set of conditional probability image [14]. The Markov chain model consists of two significant probabilities:

1) The Markov Chain-Transition probability Matrix

To predict LULC, the transition probability matrix must be calculated for the base period used in the prediction. The transition probability matrices are derived from Markov chain analysis [15].

2) The CA-Markov Chain Model (CA-MCM)

Transition models are vital especially where LULC change is driven by the factors difficult to represent mechanically such as socio-economic factors [16]. The probability of one LULC pixel change or not can be estimated through generating a probability transition matrix [14].

3.2.6 Rainfall Projection

Monthly output from the CORDEX Africa experiment was used to provide the projections and this was done for the period 2021-2050. The data was analysed on monthly timesteps, focusing on two scenarios; RCP4.5 and RCP8.5 to represent medium and high emission scenarios respectively. For evaluation of changes in the future climate, two time slices were also created: 1991-2020 (as the reference/ baseline scenario) and 2021-2050 (as the present near future / mid-century scenario). The trends were tested at α=0.05 significant level using Mann Kendall trend test. Table 7 indicates the stations used in the analysis in the area of study and their long-term trends.

ID		Rainfall		
	Stations	***tau***	**P-value**	**Remarks**
1.	Irangi Forest Station	0.026	0.333	Not Significant
2.	Kerugoya District Water Office	0.006	0.458	Not Significant
3.	Embu Met. Station	0.020	0.372	Not Significant
4.	Austrian Hut	0.018	0.382	Not Significant
5.	Mwea Irrigation Agromet Station [Thiba]	0.008	0.453	Not Significant
6.	Upper Kamweti Forest Station	0.021	0.362	Not Significant
Average		**0.020**	**0.372**	**Not Significant**

Table 7: Test of Significance in the Historical Trends of Rainfall Over Thiba River Sub Basin

3.2.7 Sensitivity Analysis (SA)

Sensitivity Analysis was conducted using the Map Removal Sensitivity Analysis (MRSA) to establish the level of influence of every variable on Ground Water Recharge (GWR). The sensitivity index, S, was computed using equation 8.

$$S = \frac{B_{map-n}}{N-1} \ldots\ldots\ldots\ldots\ldots\ldots \quad (8)$$

Where B_{map} is the base map generated through weighting all the thematic layers. N is the number of the full thematic layers used to compute the B_{map} and n is the thematic variable removed to compute sensitivity towards its removal. The bigger the variation of the random dimensionless index values from the B_{map} average index, the higher the sensitivity.

3.2.8 Verification/Validation of Groundwater Recharge Zone and Suitability Analysis

The study used production borehole depths and yields to validate the GWRS map generated. The water yields were extracted and interpolated into a raster grid using the local polynomial interpolation method. The water yields map was compared partially to the groundwater recharge potential maps.

4. Results and Discussion

4.1.1 Result Overview and Basis for Analysis

The area is constituted of three zones, the mountainous, hills and mountain foot ridges and the plain land zones covering (30.11%), 46.65%, and 23.24% of the land mass respectively [17]. High drainage density indicates low percolation thus unsuitable for recharge. Soil texture controls the percolation and infiltration of surface water into the aquifers, influencing groundwater recharge through properties such as porosity, structure, adhesion, and consistency. Clay and loam soil cover 92% and 8% of Thiba river sub basin respectively. The ranks of soils were assigned according to their degree of infiltration. Drainage density (Dd) is a measure on how the catchment is drained by streams. Dd is influenced by numerous factors, including resistance to erosion, infiltration capacity, vegetation cover, surface roughness and runoff intensity index and climatic conditions. Areas with high drainage density have less recharge rate, whereas low drainage density areas have a high recharge rate and can directly influence the groundwater recharge. These are networks such as fractures, joints and faults increase porosity and play an important role in groundwater movement and high groundwater recharge potential. While high lineaments frequency indicates very high recharge potential due to the presence of recharge pathways, low frequency does not necessarily translate into very low recharge potential. The Northeastern areas have more concentration of lineament densities. The lineaments are distributed 0-2km/km2, 2-6km/km2 and 6-15km/km2 covering 85.29%, 13.42% and 1.28% respectively. This leaves the larger area not very suitable for percolation and the most suitable area has a very steep slope compromising the available time for water to percolate [3]. This area has an indigenous forest with thick undergrowth which compensates for the resistance to flow, making it one of the vital recharge zones in the sub basin [18].

4.1.2 Rainfall and Temperature

In figure 5a all the stations exhibited two distinct seasons; March-April-May (MAM) and October-November-December (OND), where MAM records the highest rainfall amount (~300mm). OND is the second rainfall season with at least 250mm of rainfall. However, the month of September is the driest and receives less than 50mm of rainfall. In figure 5b, there are two distinct warm seasons; February-March-April and September-October-November. June-July-August (JJA) season is usually a cold season over the sub basin. Generally, the coldest month in this region is July with temperatures as low as 16.0ºC, while February, March, April, and October are warm months. This is also true since the mean average temperature also indicates that JJA is the coldest season and Sept-Oct and Feb-March are warm months/seasons. These findings confirm with several authors including who found that, rainfall in the Upper Tana basin has two distinct seasons; wet and dry, with March-May receiving more rainfall in a year over this region [19, 3,18,20].

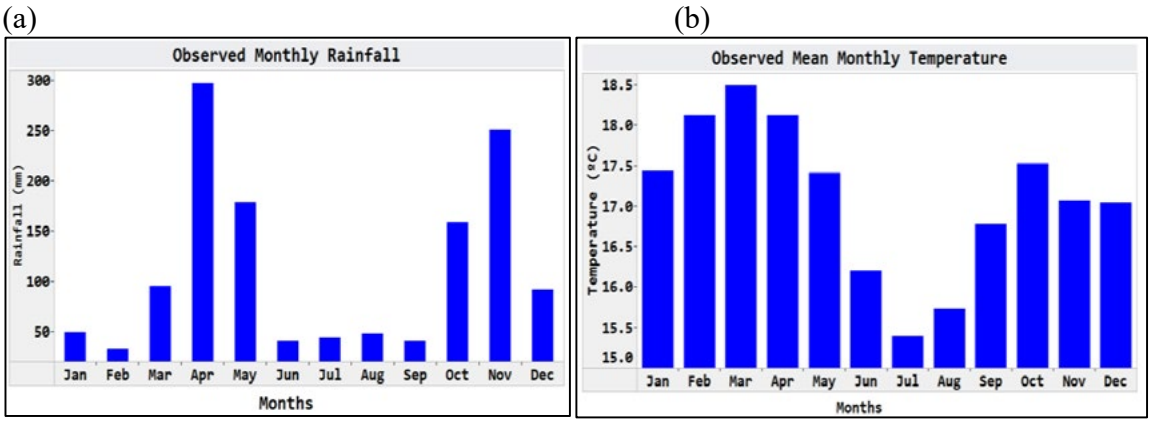

Figure 5: Monthly Means of Rainfall and Temperature Over Thiba River Sub-Basin (1986-2020)

In figure 6a, the mean annual temperature has been significantly increasing, with the maximum record observed in the year 2019 with a mean of 18.6ºC. The only cool years observed were 1986/89 and 1999 (17.4, 17.3ºC and 17.4ºC respectively). The years 2015, 2017 and 2019 were warm years had higher temperatures compared to the earlier years. The total annual rainfall (figure 6b) on the other hand has been gradually increasing with the years 1988, 1997, 2006 and 2018/19/20 receiving high amounts of rainfall (>1600mm), while the years 1996, 2000, 2004, 2017 and 2022 were dry years, with rainfall (<1000mm). Similar studies done by established that, Thiba sub catchment observed variable trends in the annual rainfall series, with significant increases in annual temperatures [18,19,21]. The long-term rainfall variations over the catchment area as a result of several factors; orographic influence from the Mt. Kenya region (Mueni, 2016), and climate indices affecting rainfall over East Africa [22,23].

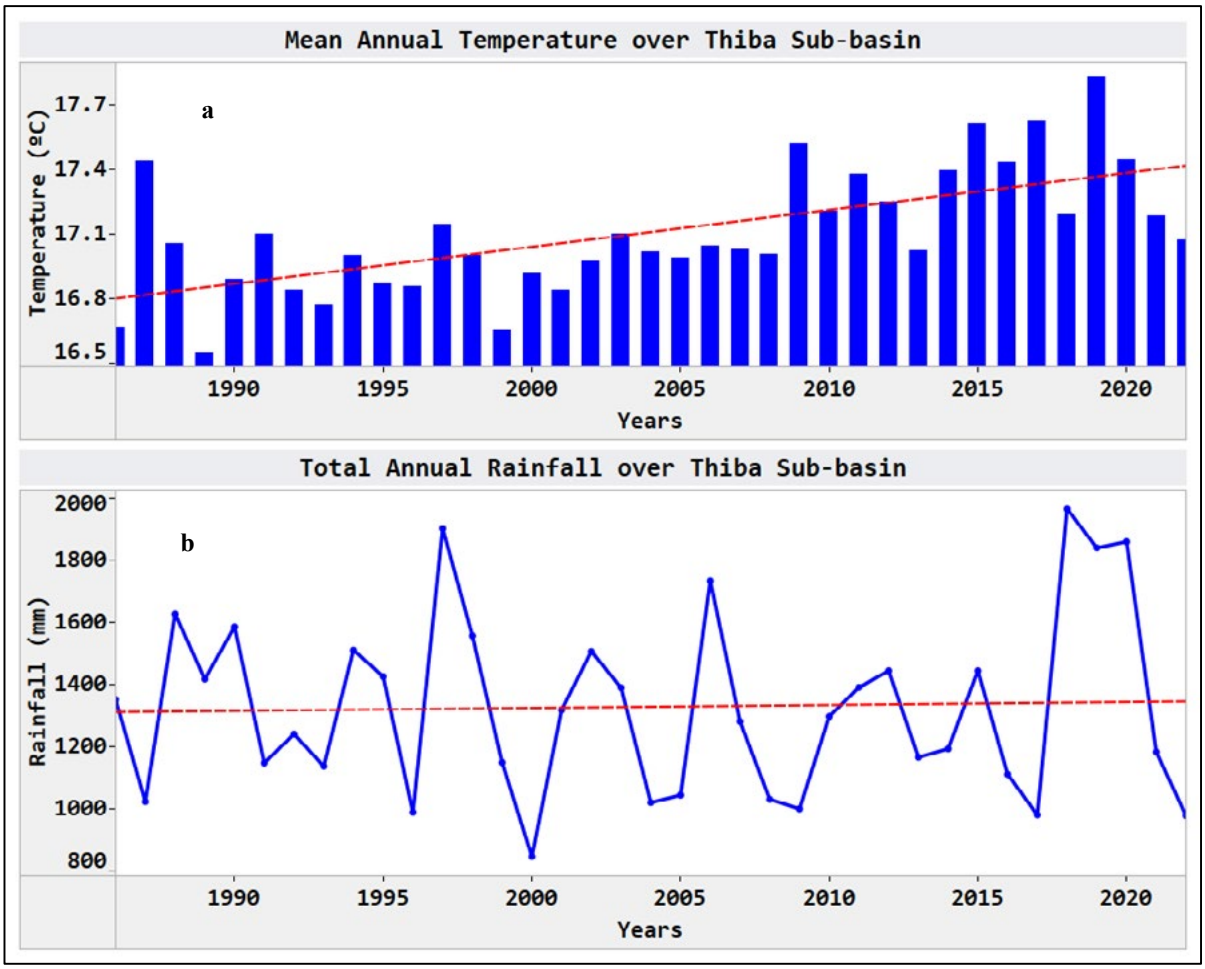

Figure 6: Mean Annual Temperature (A) and Total Annual Rainfall (B) Over Thiba River Sub-Basin for the Period 1986- 2022

In figure 7 precipitation trend shows a minimal increase in the near future. The rising temperatures and increase in evapotranspiration in the area can explain the erratic and slight increase in precipitation. The more rainfall predicted in the year 2050 especially in the middle zone can explain the increase in average recharge suitability in the middle zone.

Thiba sub catchment region has undergone several forms of droughts, meteorological, agricultural, hydrological, and socioeconomic [24]. The rising temperatures can be the cause of increased potential evapotranspiration that has triggered hydrological imbalance that led to agricultural, hydrological, and socioeconomic droughts [25]. Thiba river sub basin has faced varying levels of these forms of drought, rice fields failing due to inadequate water caused by hydrological drought. Decline in agricultural harvest triggering agricultural droughts and both contribute to socioeconomic drought. The decline in rainfall into the future can be explained by the changing micro-climate in the region, a factor associated with rapid change in land cover and increased urbanization that is increasing carbon emissions into the atmosphere.

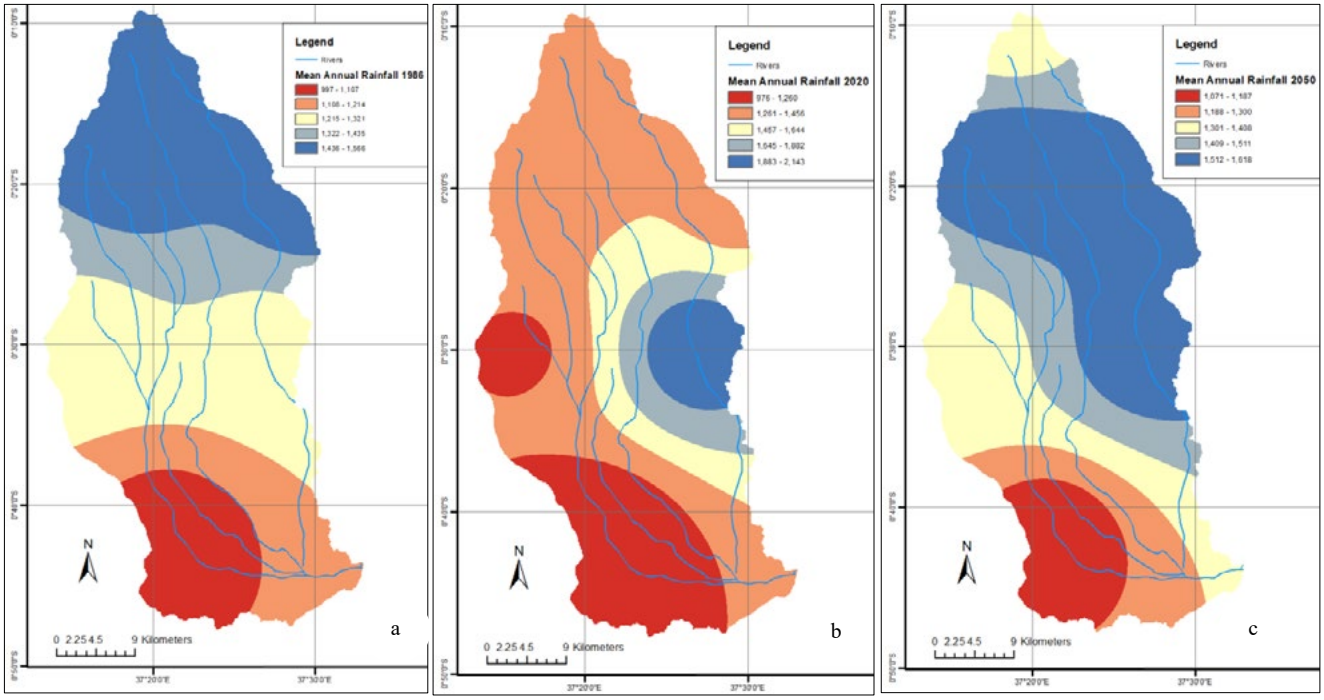

Figure 7: Rainfall Data Used in the Assessment of Groundwater Recharge Suitability 1986(A), 2020(B) and Predicted Rainfall in 2050(C)

4.2. Zonal Variable Characterization

a) Mountainous Zone

The mountain zone consists of Lineament density that varies between the three zones 6-15, 2-6 and 0-2km/km2 respectively. Lithology, consisting of grey basalts, with sparse phenocrysts of deep green olivine. Older lavas consist of extensive flows of porphyritic phonolites that lie directly on Basement System gneisses. The phonolites are associated with the brecciated phonolite. This zone has a slope rise of between 0-102%, annual mean rainfall of more than 1500mm, lithology that consists of grey basalts, with sparse phenocrysts of deep green olivine. Older lavas consist of extensive flows of porphyritic phonolites that lie directly on Basement System gneisses. The phonolites are associated with bands of brecciated phonolites. Land cover (year 2020) consists of bare land 14.6%, cropland 1.7%, Forest 82.4% and Grassland 1.2%.

Despite the density of lineaments, this landform is covered with the largest indigenous forest in the sub basin which improves the resistance to surface run off making infiltration possible. This is evidenced by the many streams that emanate from this area watering the sub basin downstream. The streams are a result of shallow sub terranean flow that meets the surface after percolation upstream. This zone has varying drainage densities ranging 0-4km/km2, 4-12 km/km2, 12-23 km/km2, 23-39 km/km2 represent 7.74%, 47.15%, 36.5%, and 8.61% respectively.

The mountain region shows favorable groundwater recharge ability. This is explained by the dense indigenous forest that cover the area creating favorable conditions for infiltration. The land in this area is also void of human activities being a gazette area thus the soil surface is stable creating a constant recharge process over a long time. Surface run-off in this area is characterized with a slow flow creating more chance for infiltration. The high mean annual rainfall also explains the availability of adequate rainfall that generates adequate run-off from which a fraction is infiltrated. The region's rainfall is predicted to increase in small margins into the near future. The current mean rainfall is on average 1453mm/yr and is predicted to increase to 1460mm/yr by the year 2050. This zone has significant lineament densities and slope variation that contribute to the water ponding which is a suitable condition for groundwater recharge.

b) Hills and Mountain Foot Ridge Zone

The hills and mountain foot ridge zone are characterized with a slope of 0-12% rise, 100% loam soil coverage, moderate rainfall of about 1250mm/yr. Land cover (year 2020) consists of cropland 87.24%, Forest 3.85% and Grassland 2.27% built up area 1.53% and insignificant bare and wetland area. The zone has varying drainage densities ranging 0-4km/km2, 4-12 km/km2, 12-23 km/km2, 23-39 km/km2, 39-65 km/km2 represent 11.9%, 47.66%, 27.42%, 12%, and 1.01% respectively.

The Suitability for recharge significantly reduced in the mountain foot ridge zone where it can be explained by the rapid conversion of land use from forest and grassland to cropland and built up. This can lead to a reduction in recharge by decreasing water retention for percolation and an increase in impermeable surfaces [26]. The middle zone of the sub basin became less suitable with the land area along the rivers being the least suitable areas. This is explained by the influence of rivers on recharge. Streams are often areas of fast stream flow and where groundwater flow meets the surface thus there is minimal percolation but external flow of groundwater. This does not rule out the ability of surface stream flow recharging aquifers in other cases where the aquifer formation allows percolation and stream flow is favorable.

The most suitable ground recharge areas increased by 2% especially in the mountain foot ridge zone, many of the suitable areas scattered in the western region of the sub basin. A reduction in more groundwater recharge suitable areas with minimal increase in most suitable groundwater recharge areas negate the extreme increase in the most suitable areas. The isolated increase in the most suitable recharge areas can be explained by the historical long-term recharge favorable conditions associated with the presence of forest cover in the middle western region of the sub basin. The long-time groundwater cycle takes to travel explains the lag period of recharge change between the clearance of the forest and improvement in suitability [27]. It is also predicted to experience more precipitation in the year 2050. This can also explain the regeneration of the recharge suitability compared to the decline in the year 2020 which is also associated with the current general decline of precipitation in rainfall.

c) Lowland/Plain Land Zone

Plain land zone is characterized by a 0-12% slope rise, rainfall of about 950mm/yr. Land cover (year 2020) consists of cropland 92.72%, Forest 0.37% and Grassland 4.41% built up area 2.26%, wetland 0.24% and no bare land. Lineament density of 2-6km/km2, lithology is made up of Banded biotite/muscovite/ hornblende gneisses; hornblende schists, granitoid gneisses. The gneisses and schists are of semi-pelitic and pelitic origin. Bands of crystalline limestone and calc-silicate gneisses occur. Clay soil with fine texture covers the plane lands and is utilized for rice farming. The zone has varying drainage densities ranging 0-4km/km2, 4-12 km/km2, 12-23 km/km2, 23-39 km/km2, 39-65 km/km2 represent 36.64%, 28.3%, 16.2%, 9.76%, and 9.09% respectively.

The region shows a rapid deterioration in the groundwater recharge suitability with the historical recharge suitability converting to moderate suitability by the year 2050. The historical dominance of grassland land cover in the areas is largely changed to cropland and built up by the year 2050 with insignificant patches of grassland. Cropland and built environment are associated with high evapotranspiration and reduction in water percolation.

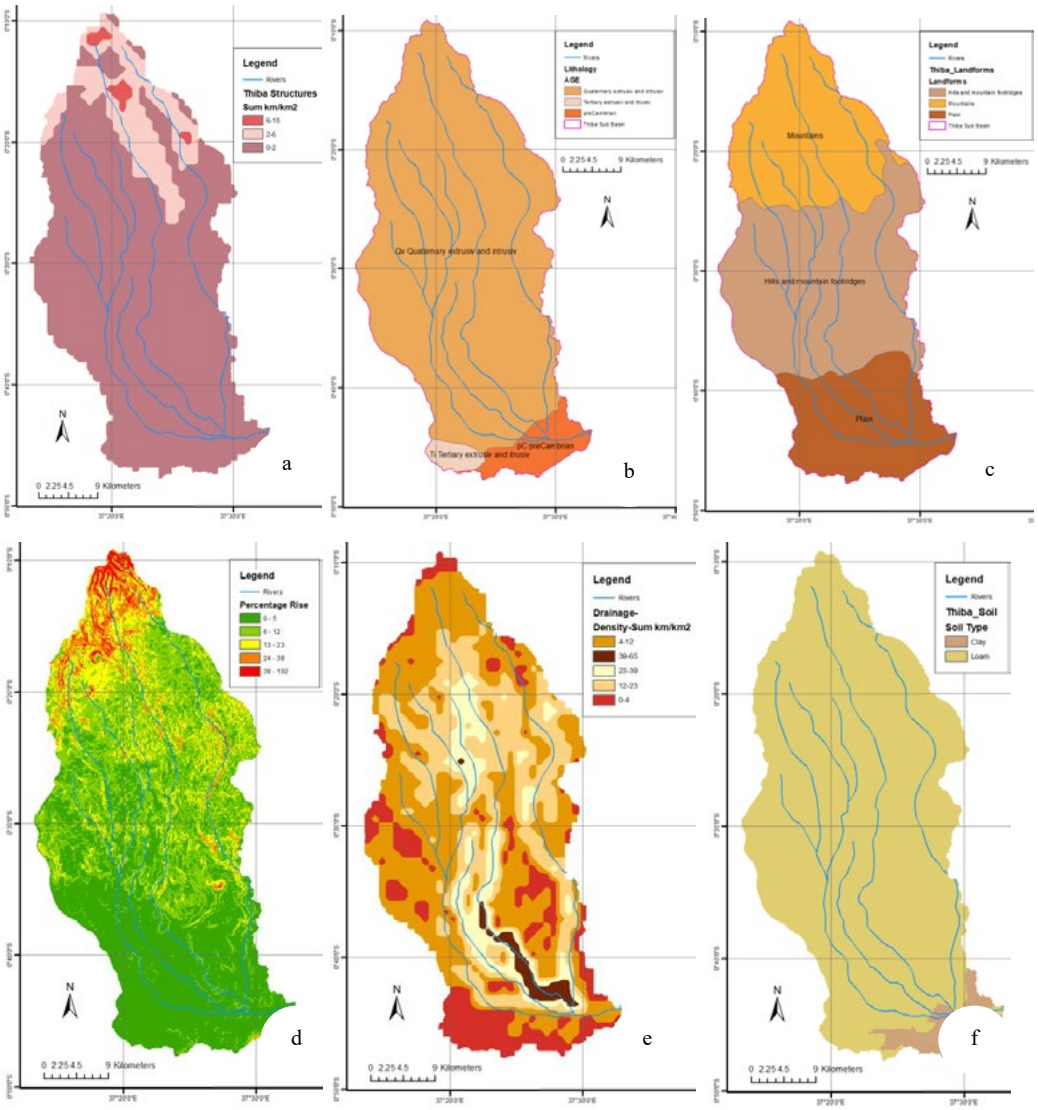

Figure 8: Data Used in the Assessment of Groundwater Recharge Suitability Lineament Density (A), Lithology (B), Landforms (C), Slope (D), Drainage Density (E) and Soil Type (F)

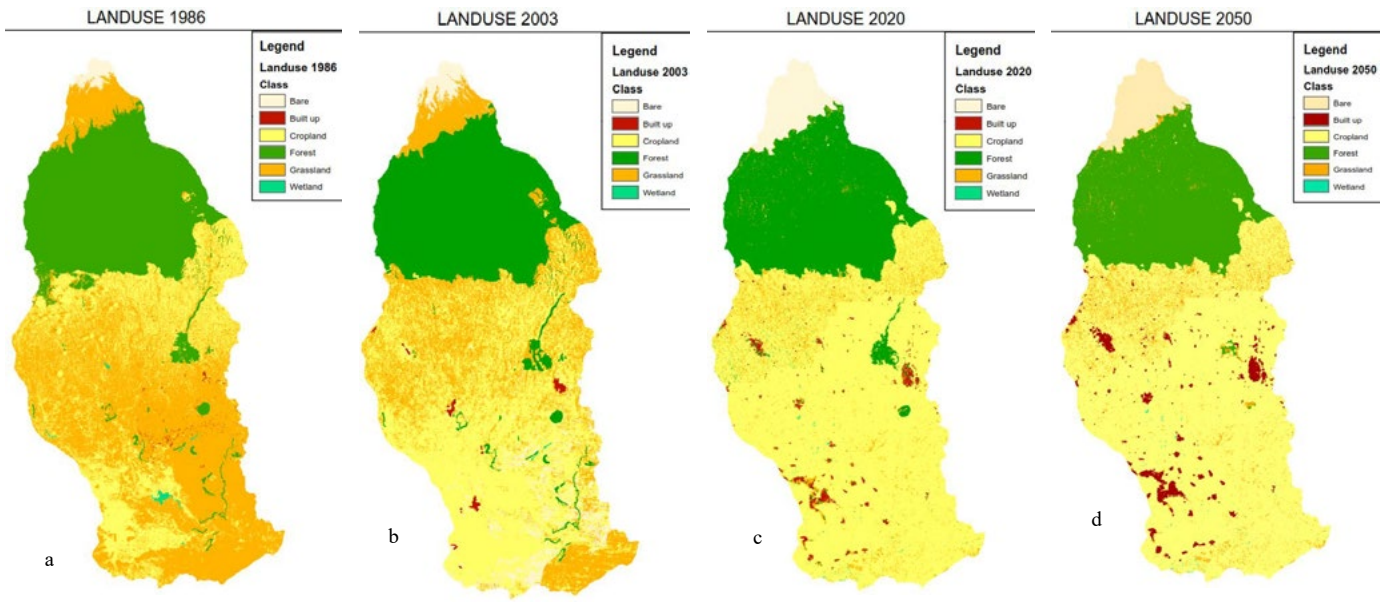

Figure 9: Land Use Data Used in The Assessment of Groundwater Recharge Suitability Land Use 1986(A), 2003(B), 2020(C) and Predicted 2050(D)

	1986	2020	2050
Class	Area (Km^2)	Area (Km^2)	Area (Km^2)
Bare	13.23	68.63	70.07
Grass land	721.34	83.84	82.79
Crop land	369.05	969.99	980.61
Forest	448.03	414.79	385.18
Built up	3.70	19.29	40.04
Wet land	3.17	1.98	0.19

Table 8: Land Use/Cover of Thiba River Sub Basin (1986, 2020 And 2050)

4.3 Ground Water Recharge

The spatial outputs of GWR suitability assessment show a spatial variation in the suitability for groundwater recharge across Thiba river sub basin. The Southwestern area of study is facing the greatest limitation of groundwater recharge suitability while the Northeastern is privileged with abundant recharge area options. The distribution of recharge suitability in the year 1986 had most, more, moderate, less, and least suitable areas constituting 14%, 30%, 32%, 20% and 5% respectively. The spatial distribution of more to most suitable areas was spatially even with the entire sub-basin indicating significant areas that had suitable rechargeability except the veins along the rivers especially in the hills foot ridges and plain zones (Figure 10a).

In the year 2020, the most, more, moderate, less, and least suitable land area represented 17.5%, 19.1%, 32.3%, 23.8% and 8.2% respectively (Figure 10b). The Suitability for recharge significantly reduced in the mountain foot ridge zone where it can be explained by the rapid conversion of land use from forest and grassland to cropland and built up. This can lead to a reduction in recharge by decreasing water retention for percolation and an increase in impermeable surfaces (Han et al., 2017). The middle zone of the sub basin became less suitable with the land area along the rivers being the least suitable areas. This is explained by the influence of rivers on recharge. Streams are often areas of fast stream flow and where groundwater flow meets the surface thus there is minimal percolation but external flow of groundwater. This does not rule out the ability of surface stream flow recharging aquifers in other cases where the aquifer formation allows percolation and stream flow is favorable.

The predicted recharge suitability for the year 2050 shows the most, more, moderate, less, and least suitable groundwater recharge areas to represent 14%, 22%, 34%, 25% and 5% respectively (Figure 10c). The most suitable ground recharge areas are predicted to decrease by 2% in the year 2050 especially

in the mountain foot ridge zone, many of the suitable areas scattered in the western region of the sub basin. An increase in more groundwater recharge suitable areas with a decrease in most suitable groundwater recharge areas negate the extreme increase in the most suitable areas.

The isolated general average increase in the moderately suitable recharge areas in the Western region of the sub basin can be explained by the historical long-term recharge favorable conditions associated with the presence of forest cover in the middle western region of the sub basin (Figure 9). The long-time groundwater cycle takes to travel explains the lag period of recharge suitability change between the clearance of the forest and improvement in suitability (Condon et al., 2021). [25].

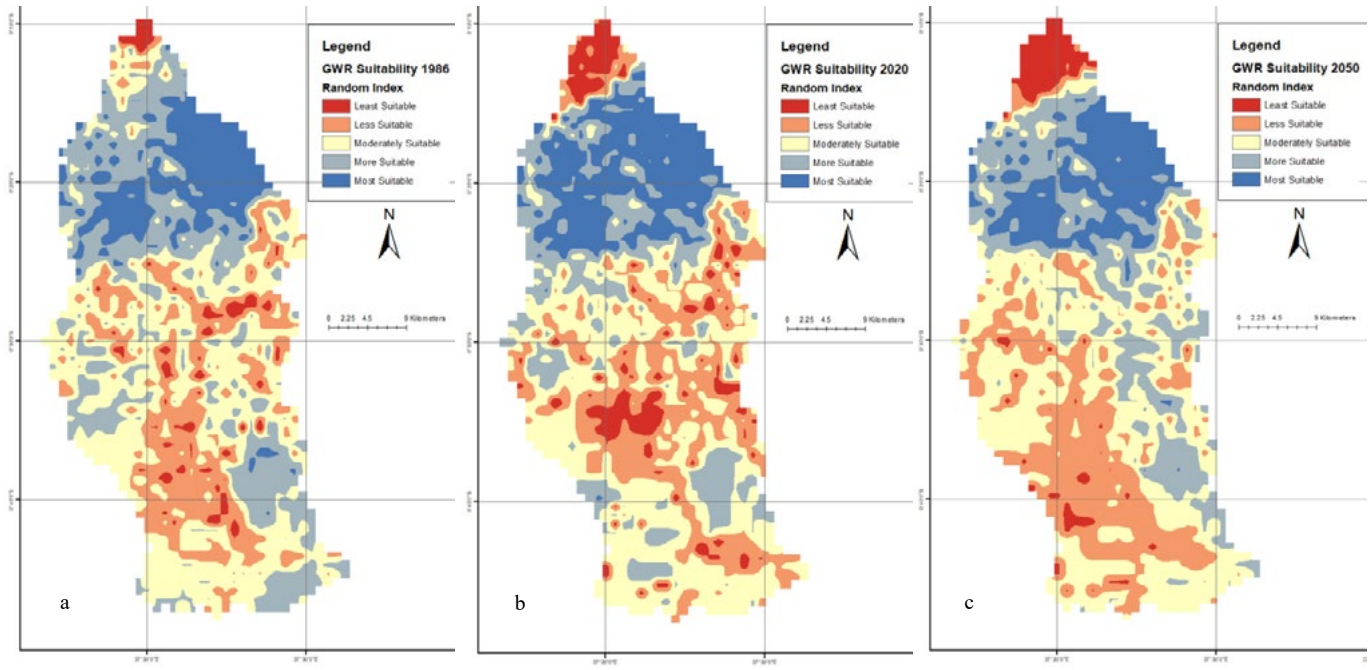

Figure 10: Groundwater Recharge Suitability for the Year 1986(A), 2020(B) and 2050(C) Prediction After Sensitivity Analysis on Parameters

The groundwater recharge suitability trend analysis shows an uncertain situation with the recharge suitability dynamically decreasing and increasing except the less suitable areas that are constantly increasing between 1986 up to 2050 (Table 9). This can be associated with the rapid uncertain trend in land use (Table 8) in the sub basin which is linked to various influences on recharge suitability.

Suitability	1986	2020	2050
Least Suitable	5	8	5
Less Suitable	20	24	25
Moderately Suitable	32	31	34
More Suitable	30	19	22
Most Suitable	14	18	14

Table 9: Recharge Suitability Percentage Area Coverage in 1986, 2020 and Predicted 2050

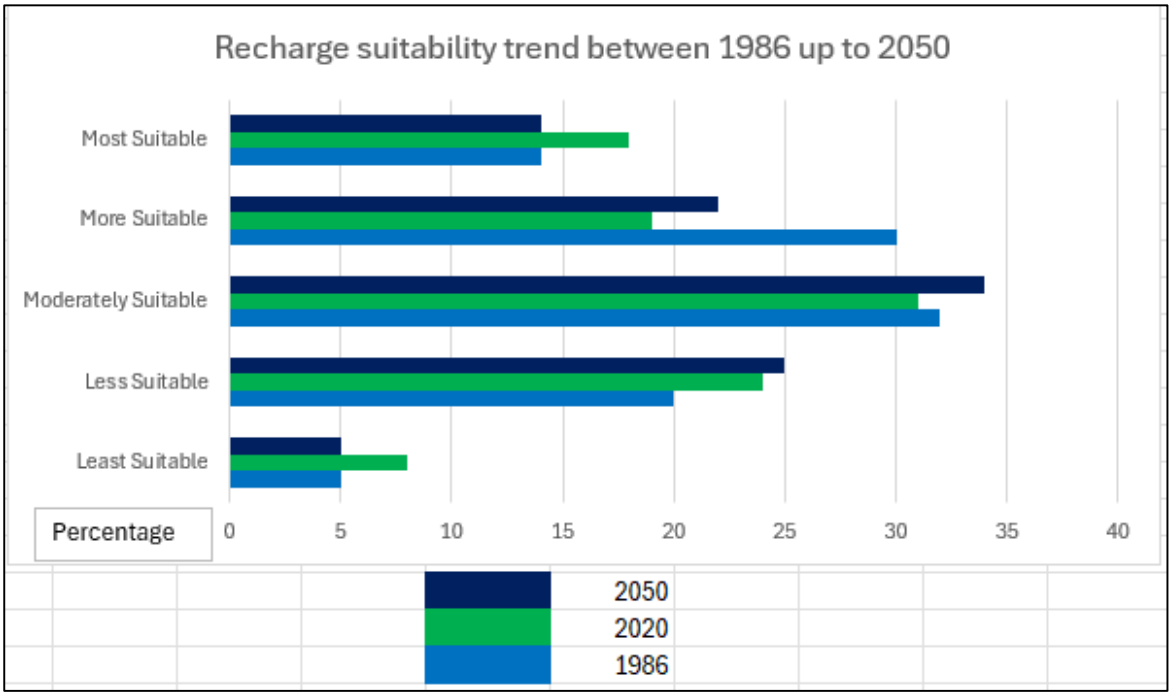

Figure 11: Groundwater Recharge Suitability Graphically Compared Between 1986, 2020 and 2050

4.4 Sensitivity Analysis

Through sensitivity analysis using the map removal method. The groundwater recharge suitability influencing variables were determined to have varying influence on the recharge. Slope, Land use, Rainfall, Lithology, Landforms, Drainage Density, Lineament density and soil were found to have high to low influence on recharge respectively (Table 10).

SENSITIVITY LEVEL						
DATA SET	**MIN**	**MAX**	**MRSA AVG**	**GWRS (8Layers) AVG**	**MRSA AVG**	**STDV**
GWRS (Sum 7layers) Less Slope	24	54	39	52.5	39	9.5
GWRS (Sum 7layers) Less Land use	28.5	51	39.75	52.5	39.75	9.0
GWRS (Sum 7layers) Less Rainfall	29.5	55	42.25	52.5	42.25	7.2
GWRS (Sum 7layers) Less Lithology	30.5	60	45.25	52.5	45.25	5.1
GWRS (Sum 7layers) Less Landforms	33.5	61	47.25	52.5	47.25	3.7
GWRS (Sum 7layers) less Drainage Density	33.5	62.5	48	52.5	48	3.2
GWRS (Sum 7layers) Less Lineament Density	36	62.5	49.25	52.5	49.25	2.3
GWRS (Sum 7layers) Less Soil	36.5	64	50.25	52.5	50.25	1.6

Table 10: Sensitivity Analysis Standard Variation Analysis on the Mean Value Between the Minimum and Maximum Random Index Range Compared to the Mean Value of the Base Map (Figure 12)

***STDV**: Standard deviation, AVG: Average, **MIN**: Minimum, **MAX**: Maximum, MRSA **AVG**: Map Removal Sensitivity Analysis Average Random Index with one layer removed, GWRS(8Layers) AVG: Map Removal Sensitivity Analysis Average Random Index with eight layers used as base map random average index

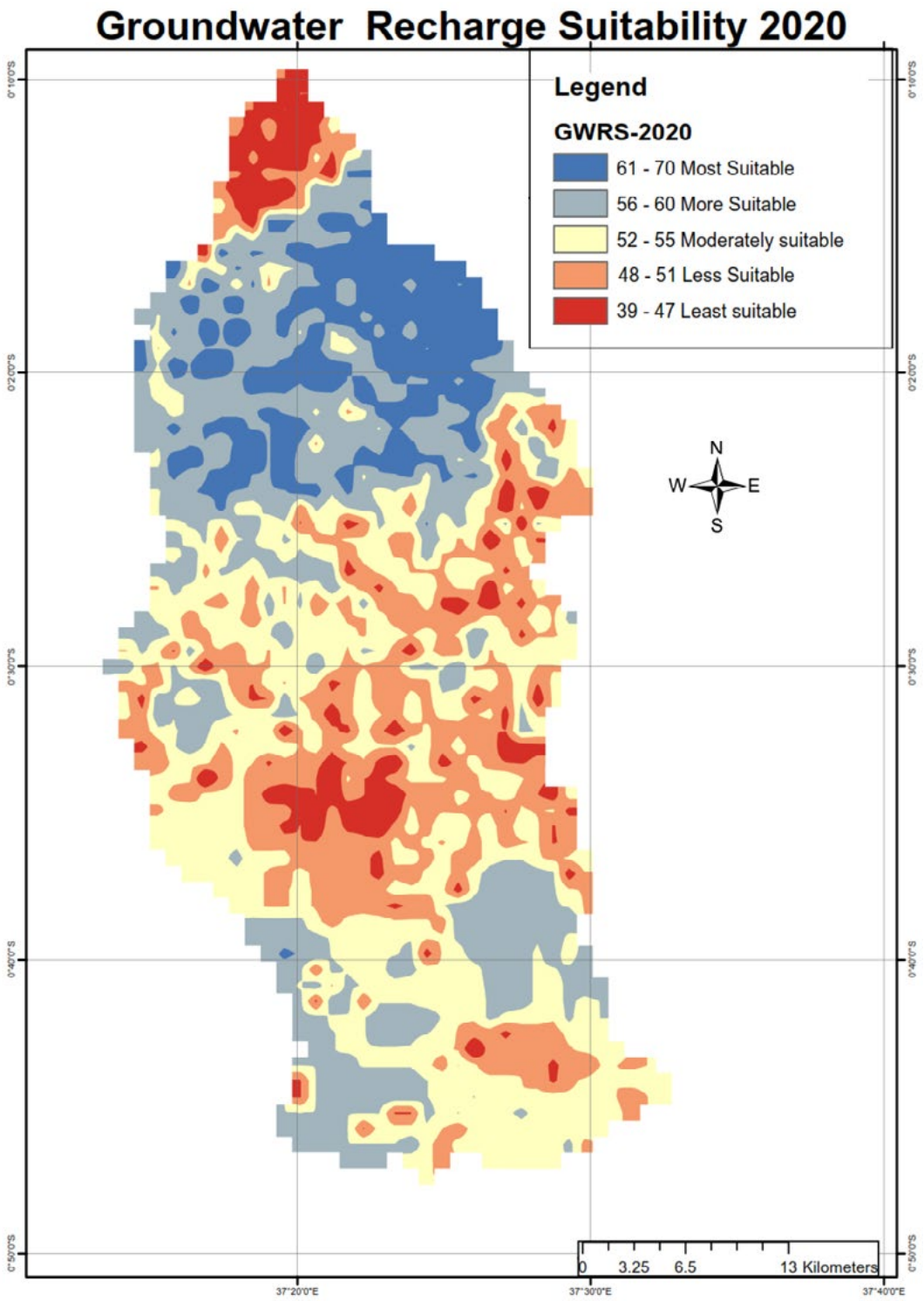

Figure 12: Groundwater Potential (2020) Base Map Before Sensitivity Analysis Using Un-Adjusted Parameter Weights

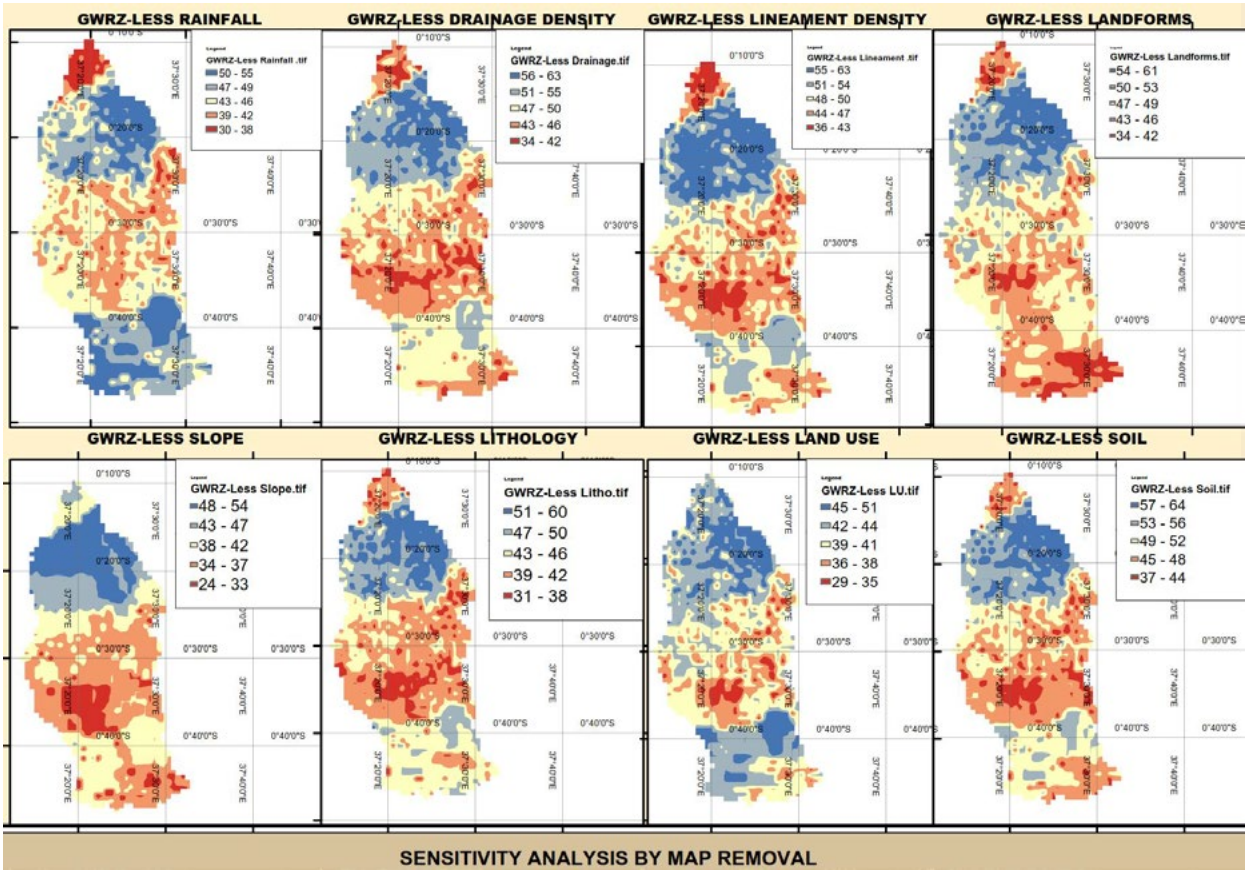

Figure 13: Map Removal Sensitivity Analysis for All the Variables Used in Gwr Assessment

4.5 Validation of Groundwater Recharge Zones

The borehole yields were rasterized based on their yields in cubic meter per day. These were done using productive borehole records obtained from the Water Resources Authority. The result shows a positive correlation between the most suitable locations and the most productive boreholes area. This phenomenon validates the recharge mapping since the study assumed that the most suitable areas for groundwater recharge are also places with high yielding boreholes (figure 14).

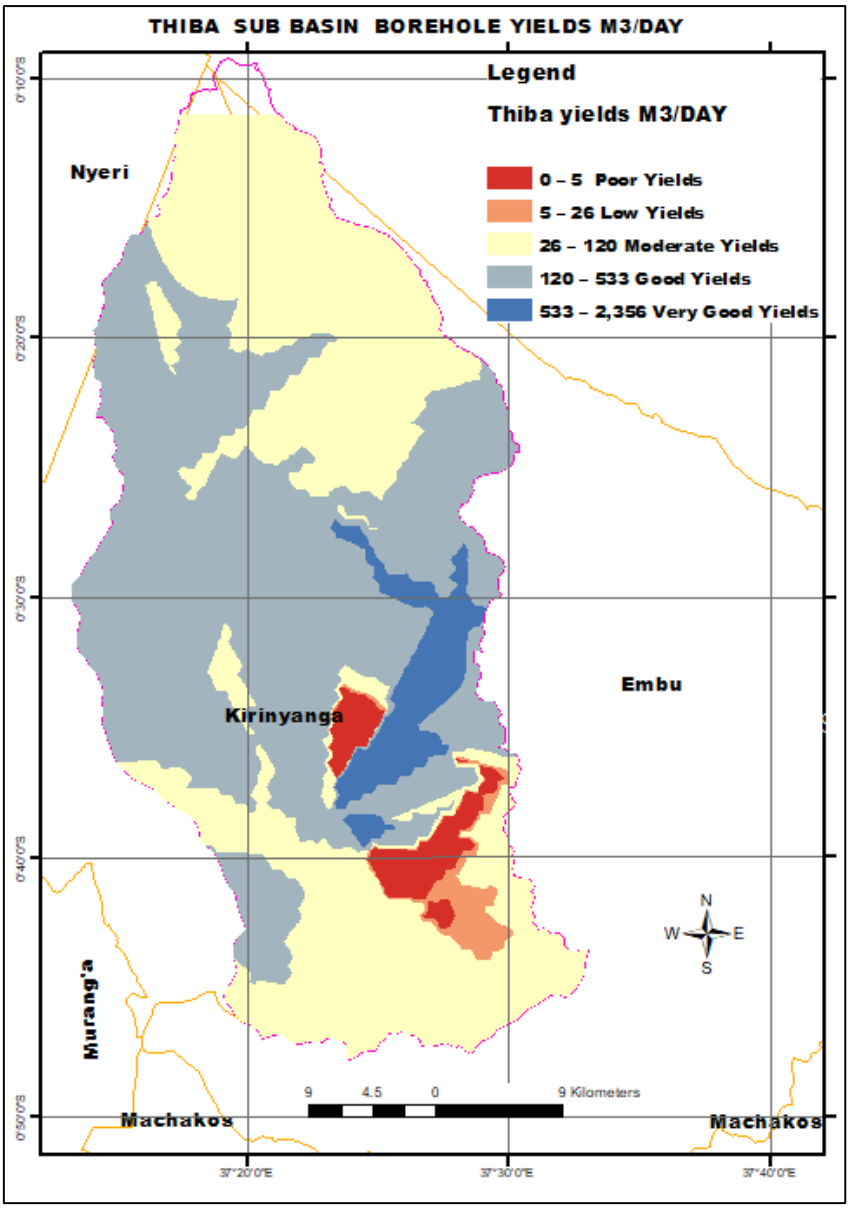

Figure 14: Water Yield Surface Map Generated from Productive Boreholes Yields in M3/Per Day

5. Conclusion

Groundwater recharge areas show significant variation in space and quantity over time when subjected to the changing land use and rainfall that was used to denote climate. Multi-Influencing Factors (MIF) technique yielded very good results in mapping the GWR suitability as an indicator of variation in groundwater potential both for abstraction and management. Temperature has been significantly increasing over the years while mean annual rainfall has been non-significantly increasing over time. This will lead to large evapotranspiration and an eventual decline in discharge in the rivers making groundwater an inevitable option. The development and sustainable management of the groundwater resources will ensure water security into the future. The larger area of the Eastern area has very good recharge potential and validation showed a potential of 25-2356m3/day yields in many areas with minor unsuitable recharge and yield areas.

Acknowledgements

I first acknowledge my Supervisors Dr. Sichangi and Dr. Makokha who supported the technical implementation of this study. I specifically thank Ruth Waswa for supporting climate data analysis, and finally my family who always supported me during the study.

Ethics Approval

This article does not contain any studies with human participants or animals performed by any of the authors.

Data Availability Statement

Publicly available datasets were analyzed in this study. The data source and description are tabulated below.

Data Types	Source
CHIRPS Rainfall (Gridded: 1981 - 2022)	https://www.chc.ucsb.edu/data
Satellite Imagery (Sentinel-2)	https://developers.google.com/earth-engine/datasets/catalog/sentinel
Climate Projections (CORDEX: Rainfall) (2006-2050)	https://esgf-data.dkrz.de/search/cordex-dkrz/

Table 11: Online Data Repositories Used as Data Sources.

Statements & Declarations

I declare that there were funds utilized during the preparation of this manuscript. The funds were from the Covenant of Mayors Sub Saharan Africa (CoM SSA) during the implementation of the Mombasa urban lab that was being implemented in Mombasa county.

Competing Interests

The authors have no relevant financial or non-financial interests to disclose.

Author Contributions

Material preparation, data collection and analysis were performed by Abel Moturi Omanga, Quincy Charles, Nashon Njoroge and Ruth Nasiroli Waswa. Dr. Valentine Ochanda, Nicolas MARQUOT and Kruti Munot commented on previous versions of the manuscript. The first draft of the manuscript was written by Abel Moturi Omanga, and all authors read, commented, and approved of the final manuscript.

Consent to Participate.

The study did not involve individuals in the study but rather use of data and modeling tools.

Consent to Publish.

No personal images needing consent for publication.

References

1. Liu, H., Kiesel, J., Hörmann, G., & Fohrer, N. (2011). Effects of DEM horizontal resolution and methods on calculating the slope length factor in gently rolling landscapes. *Catena, 87*(3), 368-375.
2. Baker, B. H., Williams, L. A. J., Miller, J. A., & Fitch, F. J. (1971). *Sequence and geochronology of the Kenya rift volcanics. Tectonophysics, 11*(3), 191-215.
3. Kasuni, S. M., & Kitheka, J. U. (2017). Modeling the impacts of land cover changes on stream flow response in Thiba river basin in Kenya. *Journal of Water Resources and Ocean Science, 6*(1), 1-13.
4. Njue, J. M., Magana, A. M., & Githae, E. W. (2022). Effects of Agricultural Nutrients Influx on Water Quality in Thiba River basin, a sub-catchment of Tana River Basin in Kirinyaga County, Kenya. *East African Journal of Agriculture and Biotechnology, 5*(1), 69-89.
5. Agwata, J. F. (2014). Spatial characteristics of drought duration and severity in the upper tana basin, Kenya. *International Research Journal of Environment Sciences, 3*(4), 18-26.
6. Bell, B., Hersbach, H., Simmons, A., Berrisford, P., Dahlgren, P., Horányi, A., ... & Thépaut, J. N. (2021). The ERA5 global reanalysis: Preliminary extension to 1950. *Quarterly Journal of the Royal Meteorological Society, 147*(741), 4186-4227.
7. Dinku, T., Funk, C., Peterson, P., Maidment, R., Tadesse, T., Gadain, H., & Ceccato, P. (2018). Validation of the CHIRPS satellite rainfall estimates over eastern Africa. *Quarterly Journal of the Royal Meteorological Society, 144,* 292-312.
8. Greenbaum, D. (1985). *Review of remote sensing applications to groundwater exploration in basement and regolith.*
9. Carlston, C. W. (1963). *Drainage density and streamflow. US Government Printing Office.*
10. Anderson, J. R. (1976). *A land use and land cover classification system for use with remote sensor data* (Vol. 964). US Government Printing Office.
11. García-Álvarez, D., Camacho Olmedo, M. T., Paegelow, M., & Mas, J. F. (2022). *Land Use Cover Datasets and Validation Tools: Validation Practices with QGIS.*
12. Zghibi, A., Mirchi, A., Msaddek, M. H., Merzougui, A., Zouhri, L., Taupin, J. D., ... & Tarhouni, J. (2020). Using analytical hierarchy process and multi-influencing factors to map groundwater recharge zones in a semi-arid Mediterranean coastal aquifer. *Water, 12*(9), 2525.
13. Kumar, S., Radhakrishnan, N., & Mathew, S. (2014). Land use change modelling using a Markov model and remote sensing. *Geomatics, Natural Hazards and Risk, 5*(2), 145-156.
14. Mishra, V. N., Rai, P. K., & Mohan, K. (2014). Prediction of land use changes based on land change modeler (LCM) using remote sensing: A case study of Muzaffarpur (Bihar), India. *Journal of the Geographical Institute" Jovan Cvijic", SASA, 64*(1), 111-127.
15. Ozturk, D. (2015). Urban growth simulation of Atakum (Samsun, Turkey) using cellular automata-Markov chain and multi-layer perceptron-Markov chain models. *Remote Sensing, 7*(5), 5918-5950.
16. Turner, M. G. (1989). Landscape ecology: the effect of pattern on process. *Annual review of ecology and systematics, 171*-197.
17. James, S., M'Ïkiugu, M. H., & Kironchi, G. (2022). Socio-Economic Factors Affecting Water Use in Lower Thiba Sub-Catchment, Kirinyaga County, Kenya. *East African Journal of Science, Technology and Innovation, 3*(4).
18. Omanga, A. M., Sichangi, A. W., & Makokha, G. O. (2023). Assessment of stream flow variability in response to the changes in climate, rainfall, and water demands: assessing stream flow variability in Thiba sub-basin. *International Journal of Energy and Water Resources, 1*-17.
19. Mueni, P. J. (2016). *Climate Change Impacts On Water Resources Over The Upper Tana Catchment Of Kenya*

(Doctoral dissertation, University Of Nairobi).
20. Atampugre, G. (2011, July). *Cost Benefit Analysis of Soil and Water Conservation technologies applicable to Green Water management in the Saba Saba sub-catchment of the Upper Tana catchment in Kenya*.
21. Langat, P. K., Kumar, L., & Koech, R. (2017). Temporal variability and trends of rainfall and streamflow in Tana River Basin, Kenya. *Sustainability, 9*(11), 1963.
22. Camberlin, P. (2018). Climate of eastern Africa. *Oxford research encyclopedia of climate science.*
23. Nicholson, S. E. (2017). Climate and climatic variability of rainfall over eastern Africa. *Reviews of Geophysics, 55*(3), 590-635.
24. Okal, H. A., Ngetich, F. K., & Okeyo, J. M. (2020). Spatio-temporal characterisation of droughts using selected indices in Upper Tana River watershed, Kenya. *Scientific African, 7,* e00275.
25. Mwendwa, P. K. (2020). *Determination of the drivers and impacts of water diversion and abstraction in selected rivers in the upper Tana basin, Kenya* (Doctoral dissertation).
26. Han, D., Currell, M. J., Cao, G., & Hall, B. (2017). Alterations to groundwater recharge due to anthropogenic landscape change. *Journal of Hydrology, 554,* 545-557.
27. Condon, L. E., Kollet, S., Bierkens, M. F., Fogg, G. E., Maxwell, R. M., Hill, M. C., ... & Abesser, C. (2021). Global groundwater modeling and monitoring: Opportunities and challenges. *Water Resources Research, 57*(12), e2020WR029500.

Copyright: *©2024 Abel M. Omanga, et al. This is an open-access article distributed under the terms of the Creative Commons Attribution License, which permits unrestricted use, distribution, and reproduction in any medium, provided the original author and source are credited.*